

# Opportunities for Shear Energy Scaling in Bulk Acoustic Wave Resonators

Sumy Jose and Raymond J. E. Huetting, *Senior Member, IEEE*

**Abstract**—An important energy loss contribution in bulk acoustic wave resonators is formed by so-called shear waves, which are transversal waves that propagate vertically through the devices with a horizontal motion. In this work, we report for the first time scaling of the shear-confined spots, i.e., spots containing a high concentration of shear wave displacement, controlled by the frame region width at the edge of the resonator. We also demonstrate a novel methodology to arrive at an optimum frame region width for spurious mode suppression and shear wave confinement. This methodology makes use of dispersion curves obtained from finite-element method (FEM) eigenfrequency simulations for arriving at an optimum frame region width. The frame region optimization is demonstrated for solidly mounted resonators employing several shear wave optimized reflector stacks. Finally, the FEM simulation results are compared with measurements for resonators with Ta<sub>2</sub>O<sub>5</sub>/SiO<sub>2</sub> stacks showing suppression of the spurious modes.

## I. INTRODUCTION

BULK acoustic wave (BAW) resonators are becoming increasingly important as the communication bands move higher into the frequency spectrum. Thin-film BAW devices are used for RF selectivity in mobile communication system and other wireless applications. We distinguish film bulk acoustic wave resonators (FBARs), in which the resonator layers are freestanding, and solidly mounted resonators (SMRs) which involve a set of reflector layers to confine the acoustic energy to the resonator layers. SMRs have the advantage of convenient processing and good heat conducting properties [1]. Another advantage of SMRs over FBARs is that SMRs provide additional degrees of freedom for design optimization [2]–[6]. There are advantages of FBARs over SMRs as well, such as a higher electromechanical coupling coefficient and fewer propagating spurious modes that must be suppressed (see, e.g., [7], [8]).

The reflector stack of an SMR must be designed for reflection of longitudinal and shear waves, because both types of waves can carry away energy to the substrate, thus reducing the quality factor  $Q$  for the main resonance of the resonator [2]–[6]. The reflection properties of a reflector stack can easily be calculated, provided that layer thicknesses and material properties are exactly known. However, in particular, experimentally determining the

shear wave transmission through a reflector stack, which is a measure for the shear wave contribution of the  $Q$  in the SMR, has been proven to be relatively difficult. For this, dedicated techniques are required, such as the laser interferometric measurement technique [9], and the resonators must be fabricated on a glass substrate [10].

Another issue is the unwanted or so-called spurious resonances evident in many practical devices. These spurious resonances are caused by the formation of higher order lateral (Lamb) wave modes for fulfilling the boundary conditions between main mode in the internal (or active) region of the resonator and the exponentially decaying displacement in the external region [11].

For suppressing spurious resonances in a resonator, the so-called frame region (FR) at the edge of the resonator was introduced [11]; see Fig. 1. The frame region, which is a mass-loaded edge of the resonator, matches the desired vibration profile in the internal region of the resonator to the vibration profile in the surroundings of the resonator (the external region).

An improvement in the  $Q$  factor for the main resonance can be observed, however, when the FR is applied to devices with shear-wave-optimized stacks. The theoretical estimation of the amount of energy stored in shear modes varies from 0.05% [12] to 1% [2]. It has been reported [5] that for best spurious mode suppression, the FR should have a width close to  $(2N + 1) \lambda/4$ , where  $\lambda$  is the horizontal wavelength of the TE<sub>1</sub> mode and  $N$  is an integer.

However, it has not yet been clarified exactly how the optimum frame region width should be determined. Furthermore, as mentioned before, determining the shear wave transmission experimentally is relatively difficult. In this work, we propose a straightforward methodology to optimize the frame region width in SMRs comprising shear-wave-optimized reflector stacks making use of FEM eigenfrequency simulations. For the first time we also demonstrate that shear wave spots, i.e., spots containing a high concentration of shear wave displacement, arise below the frame region and that the number of these spots is controlled by the frame region width. We come up with a model for the quality factor to improve the insight and address the issue of determining the shear wave transmission. Finally, some of the results are compared with experimental data obtained from resonators with dedicated Ta<sub>2</sub>O<sub>5</sub>/SiO<sub>2</sub> reflector stacks. Note that spurious mode suppression in a ZnO SMR was reported earlier [13], but with a focus on flat-amplitude mode and the coupling coefficient. In this work, our main purpose is to demonstrate the shear energy confinement and its scaling. We use an optimized frame region which is traditionally used

Manuscript received April 11, 2014; accepted June 19, 2014.

S. Jose is with Quality and Reliability, NXP Semiconductors, Nijmegen, The Netherlands.

R. J. E. Huetting is with the Faculty of Electrical Engineering, Mathematics and Computer Science (EEMCS), University of Twente, Enschede, The Netherlands (e-mail: r.j.e.huetting@utwente.nl).

DOI <http://dx.doi.org/10.1109/TUFFC.2014.006447>

to suppress the spurious modes as a tool for shear energy confinement.

This paper is outlined as follows. In Section II, we will come up with a model for the quality factor to gain more insight of the effect of the frame region width on the energy storage and loss. Section III elaborates on the methodology for the frame region width optimization. Section IV discusses the FEM simulation and measurement results and some remarks in this aspect are also highlighted. Finally in Section V, the conclusions are drawn.

## II. QUALITY FACTOR MODEL

We propose a simple analytic model for improving the insight of the shear wave contribution toward  $Q$  and hence the energy loss. With this model we will show that the method to be presented in Section III depends on device layout scaling, which in turn could influence the  $Q$ . After introducing this model, we will use the FR width as a measure to inject controlled portions of shear wave energy into the series of resonators. Finally, we will describe how the various parameters (including the shear wave reflection coefficient) can be extracted from a series of resonators.

The quality factor of the resonator with index  $m$  is related to stored energy  $E_m$  and loss  $L_m$  per cycle according to  $Q = E_m/L_m$  [4], [5]. The stored energy is a sum of longitudinal and shear wave energies stored in the resonator. The loss comprises shear wave energy and longitudinal wave energy leaking into the substrate plus acoustic energy (of both types) leaking sideways away from the resonator. Hence,  $E_m$  and  $L_m$  can be expressed as

$$E_m = E_{m,L} + E_{m,S}, \quad (1)$$

and

$$\begin{aligned} L_m &= L_{m,L,\text{sub}} + L_{m,S,\text{sub}} + L_{\text{side}} \\ &= T_L \cdot E_{m,L} + T_S \cdot E_{m,S} + L_{\text{side}}, \end{aligned} \quad (2)$$

where  $T_L$  is the transmission of longitudinal waves,  $T_S$  is the transmission of shear waves, and  $L_{\text{side}}$  is the energy loss in the external region. To determine each of the parameters, we must construct a series of resonators for which we know how the quantities  $E_{m,L}$ ,  $E_{m,S}$ , and  $L_{\text{side}}$  scale with the layout.  $T_S$  and  $T_L$  are fixed quantities for a given reflector stack.

It has been reported [5] that for the best spurious mode suppression, the FR should have a width close to  $(2N + 1)\lambda/4$ , where  $\lambda$  is the wavelength of the TE1 mode and  $N$  is a positive integer ( $N = 1, 2, 3, \dots$ ). For these particular FR widths, we know that the vibration profiles (and thus the stored energies  $E_{m,S}$  and  $E_{m,L}$ ) in the internal region are the same. Furthermore, the displacement profile in an FR of width  $3\lambda/4$  is a triple repetition of the displacement profile of the  $\lambda/4$  FR. Finally, the displacement profile of

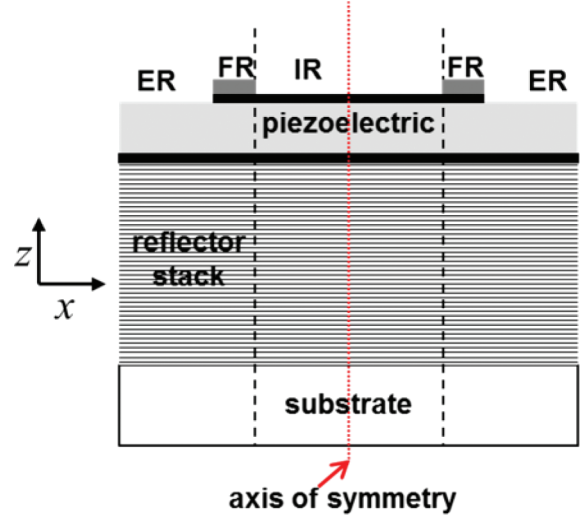


Fig. 1. Schematic cross section of the solidly mounted BAW resonator (SMR) regions: the internal region (IR), external region (ER), and the frame region (FR). Half of the device structure has been implemented in the FEM simulations using a symmetry boundary condition at the axis of symmetry.

the external region is the same for all FRs, apart from a sign. The vibration of the external region is in phase with the vibration in the internal region (IR) for  $N = 1, 5, 9$ , and exactly out-of-phase for  $N = 3, 7, \dots$ . Thus, the side-way loss  $L_{\text{side}}$  can be assumed to be the same for each of the devices.

Let us now revisit the expressions for the stored energy and the lost energy per cycle and split them up according to the regions indicated in Fig. 1. We start with a resonator series with an FR width variation of quarter wave (QW)  $(2N + 1)\lambda/4$  dimension such that the corresponding fundamental eigenfrequency is the same for the whole series. Then, the displacement profile is the same for the whole series, except for the addition of another half-sine at the outer edge. The mode profile at the outer edge of the FR is the same for the whole series as well, so the wave transmitted into the external region and the associated loss can be expected to be the same for all of them.

Under these assumptions, (1) splits according to the regions indicated in Fig. 1:

$$\begin{aligned} E_m &= E_{m,L,\text{IR}} + E_{m,L,\text{FR}} + E_{m,S,\text{FR}} \\ &= E_{m,L,\text{IR}} + \alpha_{L,\text{FR}} \cdot E_{m,\text{FR}} + (1 - \alpha_{L,\text{FR}}) \cdot E_{m,\text{FR}} \\ &= E_{L,\text{IR}} + m \cdot (\alpha_{L,\text{FR}} \cdot E_{\text{FRQW}} + (1 - \alpha_{L,\text{FR}}) \cdot E_{\text{FRQW}}), \end{aligned} \quad (3)$$

where  $\alpha_{L,\text{FR}}$  is the energy fraction of the longitudinal wave in the FR ( $= E_{m,L,\text{FR}}/E_{m,\text{FR}}$ ), and hence  $(1 - \alpha_{L,\text{FR}})$  is the energy fraction of the shear wave in the FR. The index  $m$  can be dropped from  $E_{m,L,\text{IR}}$  because the mode shape in the internal region (IR) is the same for all  $m$ , so the stored energy should be the same. Hence,

$$E_{m,\text{FR}} = m \cdot E_{\text{FRQW}}, \quad (4)$$

$$Q_m = \frac{E_{L,IR} + m \cdot (\alpha_{L,FR} \cdot E_{FRQW} + (1 - \alpha_{L,FR}) \cdot E_{FRQW})}{T_L \cdot E_{L,IR} + m \cdot (T_L \cdot \alpha_{L,FR} \cdot E_{FRQW} + T_S \cdot (1 - \alpha_{L,FR}) \cdot E_{FRQW}) + L_{side}}. \quad (7)$$

where  $E_{FRQW}$  is the acoustic energy stored in the FR when it is  $\lambda/4$  wide. Here, the resonator index  $m$  is a measure of the FR width  $W$  expressed in QW units:  $m = W/(\lambda/4)$ . Consequently, the shear wave energy stored (i.e., the shear wave spots) in the FR is described by

$$E_{m,S,FR} = m \cdot (1 - \alpha_{L,FR}) \cdot E_{FRQW}, \quad (5)$$

and scales with the QW FR width. This fact will be elaborated upon in Sections III and IV when we introduce the shear wave spot scaling.

An expression for the total loss for various  $m$  can now be written and (2) can be expanded as

$$L_m = T_L \cdot E_{L,IR} + m \cdot (T_L \cdot \alpha_{L,FR} \cdot E_{FRQW} + T_S \cdot (1 - \alpha_{L,FR}) \cdot E_{FRQW}) + L_{side}. \quad (6)$$

$L_{side}$  is expected to be equal for all  $m$ .

Because  $Q_m$  is equal to  $E_m/L_m$ , we can define  $Q_m$  using (7), see above. Eq. (7) has six unknowns:  $E_{L,IR}$ ,  $\alpha_{L,FR}$ ,  $E_{FRQW}$ ,  $T_L$ ,  $T_S$ , and  $L_{side}$ . Hence, a series of at least six resonators is required to determine each of the parameters and, therefore, also the shear wave transmission. The quality factor for each of the resonators can be extracted from measurements, and further, the six equations with six unknowns can be solved to extract the parameters, e.g., using a least-square fit. The longitudinal wave transmission ( $T_L$ ) and shear wave transmission ( $T_S$ ) determined by this method allow estimation of the effect of an optimized reflector stack. The proposed methodology, as described, assumes the displacement profiles in the IR to be the same for all of the resonators. Furthermore, it assumes that the displacement profile in the FR repeats in each section of  $\lambda/4$  width (apart from a sign). Finally, the displacement profile of the external region is the same (apart from a sign) for the whole series.

### III. FRAME REGION WIDTH OPTIMIZATION

The idea behind spurious resonance suppression using an FR is that it matches the boundary condition for a homogenous excitation in the internal region and the exponentially decaying tails in the area outside the resonator. The optimal width of the FR is close to a quarter-wavelength of the TE1 mode usually visualized in the dispersion curve [5].

The traditional way of obtaining the dispersion curve is to employ harmonic analysis from simulation. However, in this work, we propose an eigenmode analysis on fully FR covered finite-sized resonators with large discontinuities at

their edges. FEM eigenfrequency simulations facilitate the direct construction of the dispersion curves from the discrete eigenfrequency points. By using symmetry boundary conditions in FEM simulation settings, eigenmodes automatically fulfill three boundary conditions: 1)  $u_z \neq 0$ , 2)  $\partial u_z / \partial x = 0$ , and 3)  $u_x = 0$ , with  $u$  being the displacement and  $x$  and  $z$  being the horizontal and vertical directions, respectively. We make use of this property to extract the eigenfrequencies from FEM eigenmode analysis to plot the dispersion curves.

For a practical finite BAW resonator, dispersion curves are formed by discrete points on a smooth continuous line. The discrete points on the dispersion curves that form trapped standing wave resonances within the resonator width  $W$  can be determined in terms of the lateral wave number  $k_x = m\pi/W$ , with  $m = 1, 2, 3, \dots$  representing the modes [13], [14]. The frequencies of these modes,  $f = f(k_x)$ , can be determined from 2-D eigenfrequency simulations to plot a dispersion curve.

Starting with an educated guess of the FR width, i.e. one-quarter wavelength, in the simulations, the width can be further optimized for spurious suppression and wave confinement. To do so, two different dispersion curves must be constructed from eigenmode analysis, each using the symmetry plane in 2-D FEM: a dispersion curve originating from a resonator comprising the IR and external region only, and a second dispersion curve from a resonator comprising the FR, i.e., the mass-loaded (edge of the) resonator, and the external region (ER), see Fig. 2. Both resonators have the same reflector stack and resonator thickness.

The 1-D resonance frequency (TE1 mode)  $f_{R,1D}$  of the IR and the mass-loaded FR have been verified from the impedance curves using 2-D FEM harmonic analysis, because the FEM simulations also depend on the meshing (which could cause numerical noise) and models. We verified the results with our 1-D Mason model calculations, showing good agreement. Because the dispersion is of type I, the dispersion curve of the resonator will have a positive slope [2], as shown in Fig. 3.

Then, the wave number is taken from the dispersion curve of the mass-loaded resonator, corresponding to the  $f_{R,1D}$  of the resonator comprising the IR and external region only. The particular  $W$  of the mass-loaded resonator corresponding to  $f_{R,1D}$  can then be calculated from the  $k_x$  value corresponding to  $x$ -axis intercept  $k_x = 2\pi/\lambda = \pi/(W)$  (with  $m = 1$ ), and consequently the obtained  $W$  equals  $\lambda/4$ , refer to Fig. 3. Then, this eigenmode for the mass-loaded resonator (FR and ER) may be combined with the 1-D mode of the internal region to form a constituted eigenmode at  $f_{R,1D}$ .

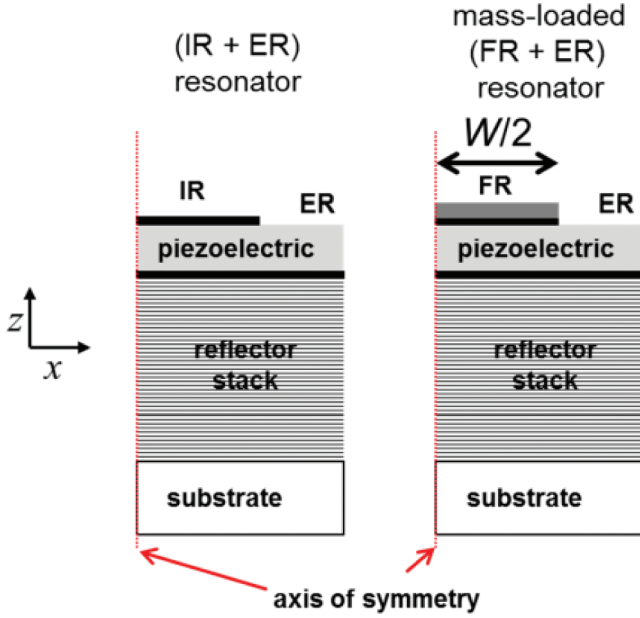



Fig. 2. Schematic cross sections of the resonators used in the 2-D FEM eigenmode analysis for the frame region optimization: (left) the resonator comprising an internal region (IR) and external region (ER) only, (right) the mass-loaded resonator comprising the frame region (FR) and ER only. Half of the device structure has been implemented in the 2-D FEM simulations using a symmetry boundary condition at the axis of symmetry. Therefore, half the resonator width ( $W/2$ ) is used and, consequently, for the actual lateral wave number, we should multiply the width by a factor of 2. 

In FEM simulations, the displacement profiles or vibration maxima against the position in an SMR with an optimized frame region width  $W$ , shown further in Section III, can be divided into longitudinal motion and horizontal (shear) motion. The difference between those can be distinguished inside the simulation tool so that we can pinpoint whether we observe shear or longitudinal motion (as shown in Figs. 6 and 7, discussed in Section IV). In addition, the reflection of the type of waves depends on the reflector stack underneath the resonator. For instance, in the case of shear waves, these are reflected by our optimized reflector stack, as predicted by our 1-D calculations reported in our earlier work [6] (see, e.g., Fig. 1). Furthermore, we analyzed the displacement plots using the longitudinal and shear energy velocities in 1-D simulations and compared it with 2-D FEM simulations showing good agreement. This analysis confirmed the shear vibration which translates into the so-called shear-confined spots.

It is assumed that in the internal region there is only vertical displacement (as demonstrated with FEM simulations in Figs. 6 and 7). Now, below the frame region, in the top oxide layer, there is a strong spot of horizontal motion, i.e., shear wave motion [6], [15]. If the reflector had poor reflection properties for shear waves, then the shear-wave energy stored in this spot would leak into the substrate and there would be an overall decrease in  $Q$ . For a large device however, the decrease in  $Q$  is hardly visible because the amount of energy stored in this spot is very small as compared with the energy in the internal region,

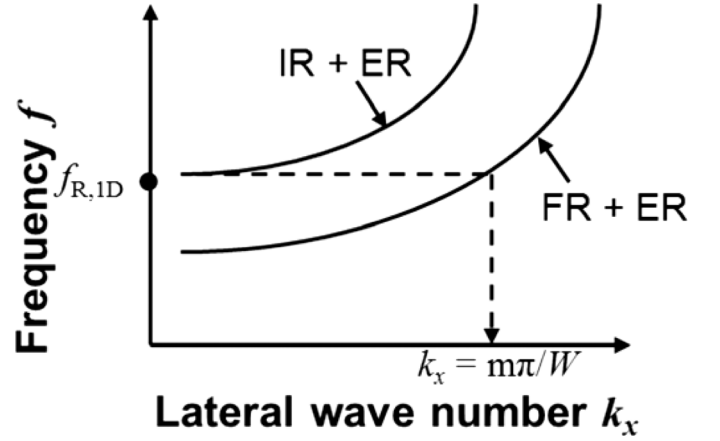


Fig. 3. Illustration of the optimization method. The top and the bottom dispersion curves correspond to the curve of, respectively, the resonator comprising an internal region (IR) and external region (ER), and the one with a frame region (FR) and ER (i.e., the mass-loaded resonator). The vertical dashed line indicates the  $k_x$  value corresponding to the  $x$ -axis intercept, from which the quarter-wavelength frame region can be calculated ( $m = 1$ ).

as can be found in the model discussed in Section II. For a small device, change in  $Q$  will be more pronounced, and hence a shear-optimized reflector can be differentiated from a poor shear wave reflector. However because such a good shear-optimized reflector has sacrificed reflectivity for longitudinal waves, it is difficult to distinguish whether a change in  $Q$  is due to changed longitudinal reflectivity or changed shear-wave reflectivity. Therefore, we propose a possible methodology to experimentally determine longitudinal and shear wave transmissions using the principle of shear energy scaling.

We propose to make a series of resonators with frame region widths  $QW$ ,  $3QW$ ,  $5QW$ , etc., up to  $11QW$  or more. All these frame regions will support 1-D motion (i.e., longitudinal motion only) in the internal region. At the same time, the shear wave motion scales with the frame region width, see (5). This is illustrated in Fig. 4: a growing number of shear spots will be seen when stepping to the next odd multiple of a quarter wavelength. As the number of frame region widths increases, more energy will be lost as shear energy in the frame region area. Hence, a reflector stack with poor shear wave reflection will suffer from a drop in  $Q$  as FR width increases. On the other hand, in the resonator series with shear-optimized reflector stacks,  $Q$  will be more or less the same for the whole resonator series [5].

#### IV. FEM SIMULATION AND EXPERIMENTAL VERIFICATION

We verified the methodology described in Section III by harmonic analysis in Comsol FEM simulations (Comsol Multiphysics, v. 3.5, Comsol Inc., Burlington, MA) for two different resonators with each having a different shear-wave-optimized reflector stack [15]. One is an aluminum

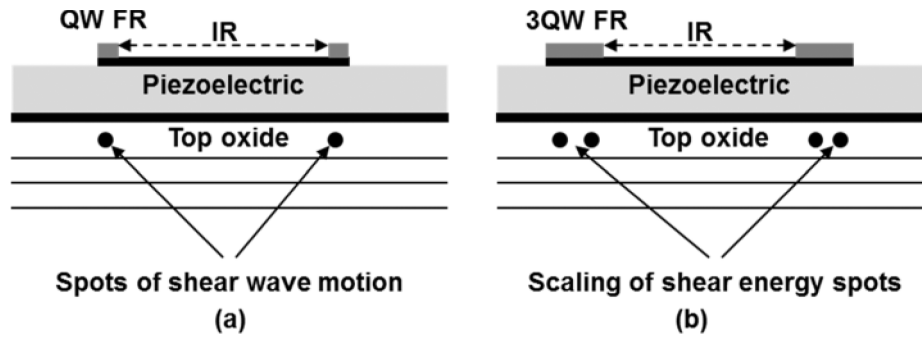


Fig. 4. A schematic illustration of (a) shear-energy spot (or shear energy confinement) and (b) scaling of the shear-energy spots by varying the quarter-wave frame region width. In this exercise, the internal region (IR) is kept constant and the frame region (FR) extends outwards. A growing number of shear spots will be observed when stepping to the next odd multiple of a quarter wavelength.

nitride (AlN)-based SMR with a  $\text{SiO}_2/\text{Ta}_2\text{O}_5$  reflector stack, for which we verified the optimum frame region widths in experiments, as will be shown later. The AlN film is a dispersion type-II layer; however, the reflector stack is chosen such that we obtain dispersion type-I behavior. The second resonator is a zinc-oxide (ZnO, type I)-based SMR with a  $\text{W}/\text{SiO}_2$  reflector stack.

A 2-D FEM physical model of the SMRs with varying quarter-wave frame region widths were simulated to verify the scaling of shear spots. Half-structure simulations were done, applying symmetry boundary condition ( $u_x = 0, \partial u_z / \partial x = 0$ ) at the center of the device. The only discontinuous layer is the top electrode (with free edge boundaries). At the right-hand edge of the devices, free boundary conditions with absorbing edges were defined to avoid generation of standing waves resulting from the reflection at the side of the resonator. To avoid the reflections from the substrate, a Rayleigh damping condition was applied to the substrate layer.

Starting with the frame region width obtained using the optimization method, i.e., around  $5 \mu\text{m}$ , the 2-D FEM physical model was constructed with a series of QW frame region widths. Note that this SMR is an AlN (type II)-based SMR, and to make the dispersion type I, we modified the top oxide layer thickness [6]. Further, the resonator has a 9-layer  $\text{SiO}_2/\text{Ta}_2\text{O}_5$  optimized reflector stack [12] at 1.88 GHz. A silicon nitride frame of 40 nm thickness was used.

The dispersion curves of the device with and without a frame region are shown in Fig. 5. Because of the mass loading, the dispersion curve of the former has been shifted downwards and its dispersion branch is not exactly parallel [17]. By mass loading, another material is added into the stack, yielding different properties. The results show that a frame region width corresponding to  $5.37 \mu\text{m}$  is required to match the resonance frequency of the internal region, i.e., corresponding to one-quarter wavelength.

Fig. 6 shows the simulated displacement profiles of longitudinal (vertical motion) and shear (horizontal motion) waves at the resonant frequency for an SMR with varying quarter-wave frame region widths QW ( $5.37 \mu\text{m}$ ), 3QW ( $16.11 \mu\text{m}$ ) and 5QW ( $26.85 \mu\text{m}$ ). While varying the

frame region width, the internal region is kept constant and the frame region extends outwards.

The figure shows that the longitudinal profile in the internal region remains almost the same for all three cases. In the frame region, the longitudinal energy scales. Looking at the shear displacement profile, a growing number of shear spots is observed when the frame region width is varied with an odd multiple of a quarter wavelength. This is a clear indication of the scaling of stored shear energy [see (5)]. It can also be seen from the figure that in the external region, the energy loss at the edge is not the same for all three cases, it seems to be scaling with  $(2N + 1) \cdot \text{QW}$ . The energy loss meant here is the energy loss from the resonator to the external region, which is seen as displacement indications in the plot in the external region. Looking at the plot, one can see that external region displacement is decreasing when going from QW to 3QW to 5QW. This can, however, be attributed to the mesh-

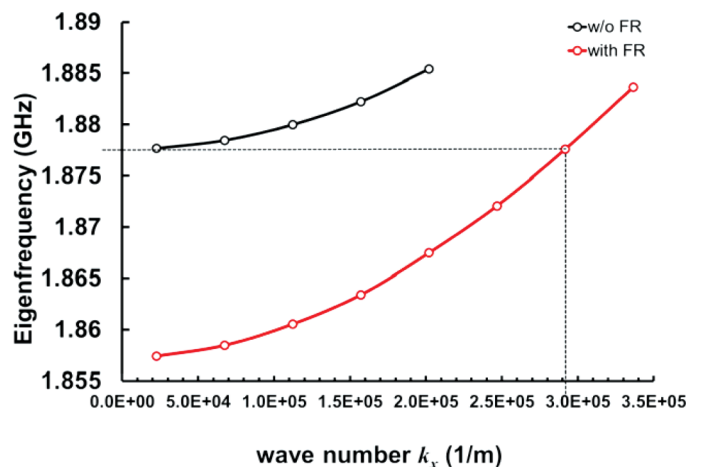


Fig. 5. Dispersion curves obtained from 2-D FEM eigenfrequency calculations for an AlN SMR with a 9-layer  $\text{SiO}_2/\text{Ta}_2\text{O}_5$  optimized reflector stack at a resonance frequency of 1.88 GHz. The black line is the curve for the device without a frame region, the red line is for the device with a frame region. The horizontal dashed line indicates the resonance frequency ( $f_{R,1D}$ ) at a lateral wavelength of  $k_x = 0 \text{ 1/m}$  (zero per meter) for the former. For matching this frequency, a frame region width corresponding to  $k_x \approx 2.92 \cdot 10^5 \text{ 1/m}$  is required, i.e.,  $W \approx 5.37 \mu\text{m}$ .

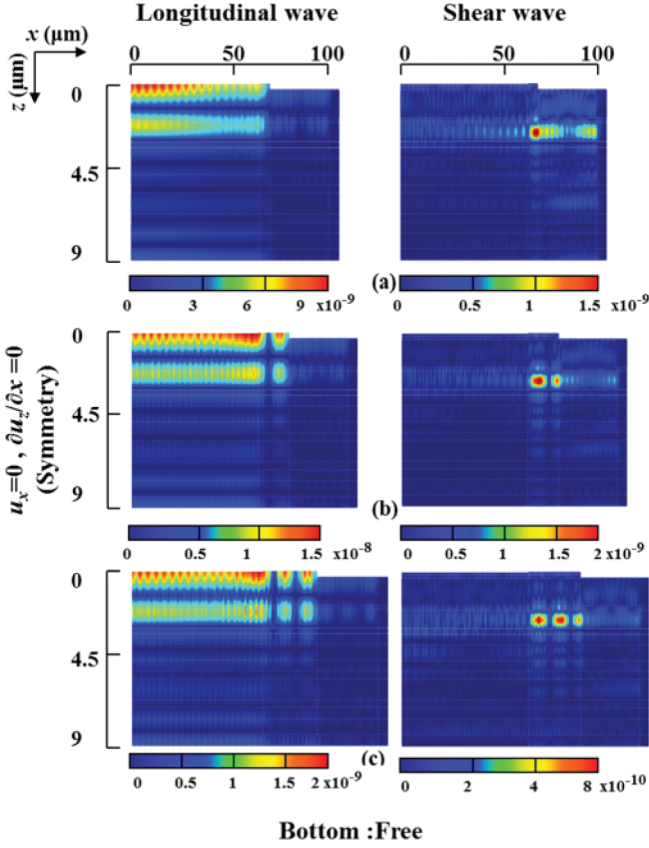


Fig. 6. 2-D FEM results of the vertical displacement of longitudinal waves (vertical motion, left) and shear waves (horizontal motion, right) at resonant frequency  $f_R \approx 1.88$  GHz of an AlN-based SMR with a 9-layer  $\text{SiO}_2/\text{Ta}_2\text{O}_5$  reflector stack designed for various optimized quarter-wave frame region widths (a) 1QW ( $5.37 \mu\text{m}$ ), (b) 3QW ( $16.11 \mu\text{m}$ ), and (c) 5QW ( $26.85 \mu\text{m}$ ). The internal region (IR) is kept constant and the frame region (FR) extends outwards. The number of shear spots scales with the odd multiple of QW frame regions. Boundary conditions at bottom and top are assumed to be free of stress. Absorbing boundaries were used at the right-hand side.

ing refinement and/or damping parameter applied in the absorbing boundary condition.

We have also verified the scaling of the shear spots in a ZnO (type I)-based SMR with a 5-layer  $\text{W}/\text{SiO}_2$  reflector stack with 2-D FEM simulations. The optimized quarter-wave frame region determined for this resonator was  $5.35 \mu\text{m}$ . The resonator is designed to operate at 1.96 GHz with an optimized reflector stack [12], [16]. The frame thickness used here was 85 nm.

The simulated displacement profiles of longitudinal and shear waves at the resonant frequency with varying QW frame region widths are shown in Fig. 7. In this case, the optimized frame region has not yet resulted in a flat longitudinal mode. This can be reached by further tailoring the layers in the external region and then adapting the optimization method. For the shear wave scaling to work, the flat amplitude mode is not a necessary criterion, because with a near-quarter FR we can already see the shear wave confinement. Of course, the flat amplitude mode is required for improving the coupling coefficient, but that

is not a part of this work. The longitudinal profile in the internal region, on the other hand, remains the same for all three cases. Below the frame region, the longitudinal energy again scales. The energy loss in the external region remains almost the same.

It is interesting to note the encroachment of shear energy into the resonator layers. For the ZnO resonator, the amount of shear energy spots also scales with the varying frame region width, as in the AlN resonator. However, this also holds for the shear energy in the piezoelectric layer below the frame region, which was not observed in the AlN resonator. We think that the presence of shear energy in the active resonator area is attributed to the use of the type-I piezoelectric material. In our earlier work [6], we reported that this effect was also visible in a simple piezoelectric slab with electric boundaries for the electrode, i.e., FBAR, and hence that it is independent of the reflector stack.

For verification, we carefully checked the stored energy values in the case of the ZnO resonator with the shear-wave-optimized  $\text{SiO}_2/\text{W}$  stack which shows no leakage in the external region. These FEM simulations were done with a frequency resolution of 0.5 MHz and a  $0.5 \mu\text{m}$  mesh size. We extracted stored energy values from the results for various FR widths up to 11QW. The results show that the stored energy in the active region is around 1.1 mJ and the  $Q$  values of 3275 obtained with the 3-dB bandwidth method remain almost constant up to 7QW. Although the multiple QW lengths allow the shear energy scaling, the reflector stack below offers a good shear reflection, and hence  $Q$  remains mostly unchanged. The slight variation of the stored energy across various FR widths can be attributed to numerical noise caused by meshing or rounding errors for the frame region width for higher multiples. This has affected especially 9QW and 11QW.

As mentioned earlier, the focus of this work is to demonstrate shear energy scaling. The quality factor model treated in Section II is to elucidate one possible application of this method. Together with the  $Q$  dependency of frame region, one could also investigate the dependence of the coupling coefficient on variation of frame region width; however, that is beyond the scope of this paper.

For the frame region optimization, the FEM results have been verified experimentally. Fig. 8 shows a comparison between the measured and FEM-simulated impedance curves for a resonator with and without a frame region of  $5 \mu\text{m}$ . For completeness sake, the phase curves of the same devices are shown in Fig. 9. The  $5 \mu\text{m}$  frame region in the experiments is not exactly at the optimum of  $5.37 \mu\text{m}$ , although it suffices to show the trend. In both the simulations and experiments, a significant reduction of the spurious modes in the impedance curve is observed near the antiresonant frequency in the case of the resonator with an FR, indicating the reduction of acoustic losses [5]. This also confirms that the optimized frame region works well with the shear-optimized reflector stack design approach. The frame region has been employed by the industry that

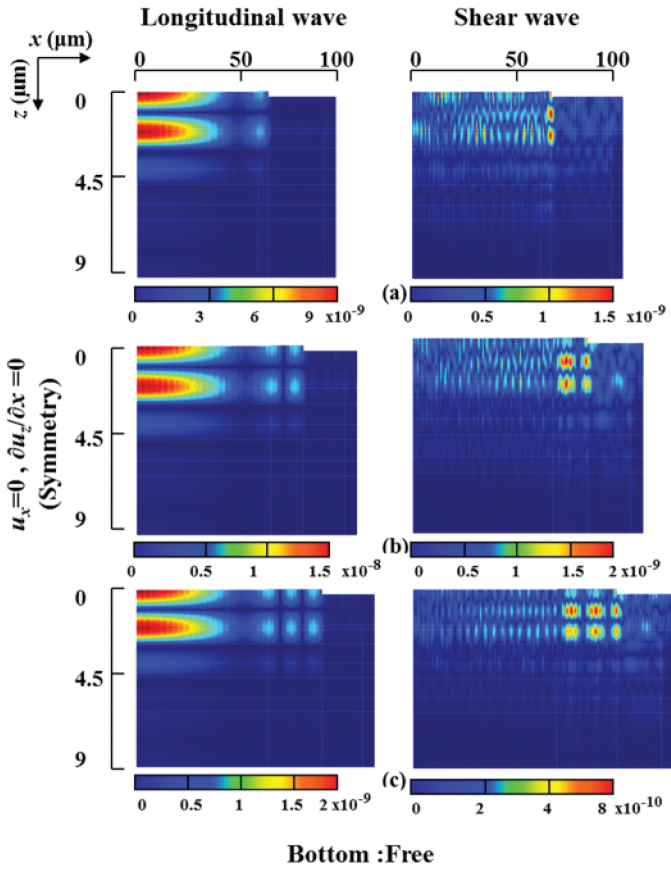


Fig. 7. 2-D FEM results of the vertical displacement of longitudinal waves (left) and shear waves (horizontal motion, right) at resonant frequency  $f_R \approx 1.96$  GHz of a ZnO-based SMR with a 5-layer  $\text{SiO}_2/\text{W}$  reflector stack designed for various optimized quarter-wave frame region widths (a) QW ( $5.35 \mu\text{m}$ ), (b) 3QW ( $16 \mu\text{m}$ ), and (c) 5QW ( $26.75 \mu\text{m}$ ). The internal region (IR) remains constant and the frame region (FR) extends outwards. The number of shear spots scales with the odd multiple of QW frame regions. Boundary conditions at bottom and top are assumed to be free of stress. Absorbing boundaries were used at the right-hand side.

has been selling filters using frames and shear wave reflectors for around 10 years. Note that the main resonance peak shift in the experiments between resonators with and without the FR could possibly be attributed by the process spread.

## V. DISCUSSION

There are some important remarks to be made about the proposed methodology. This methodology relies on the fact that the locations of longitudinal motion in the internal region and shear motion below the frame region can be split. This is achieved by an optimized frame region width on a type-I dispersion layer stack. For a type-II dispersion, 1-D motion can be achieved in the internal region using a recessed region (mass removal) rather than a frame region (mass loading). According to the theory [11], one should then mass load the external region heavily. The latter has the practical problem that it requires a dielectric that is

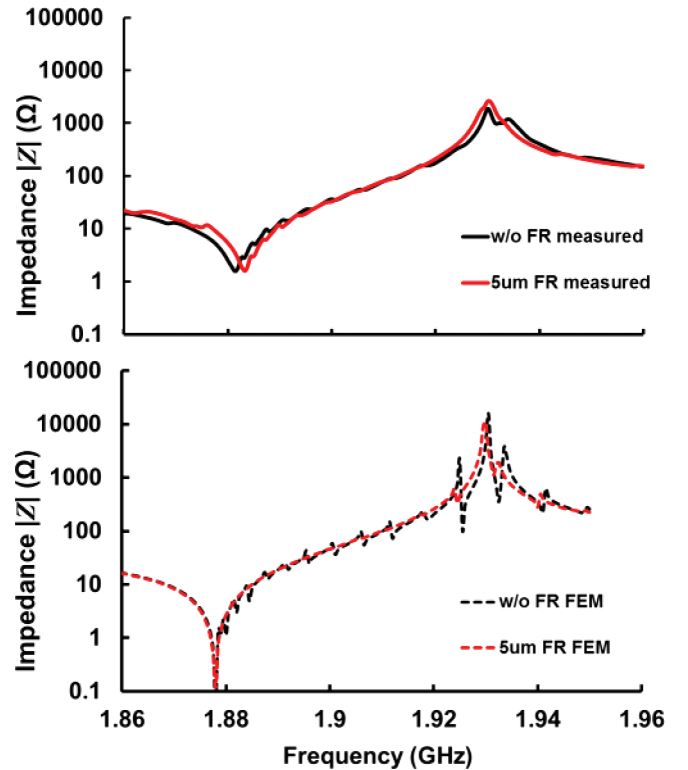


Fig. 8. Comparison of impedance curves from measurements (top) and the Comsol model (bottom) in an SMR with an optimized reflector stack with and without an FR of  $5 \mu\text{m}$ . The spurious resonances are suppressed with the optimized frame region width both in the simulations and in the measurements. The active device area is  $150 \times 150 \mu\text{m}$ .

very heavy, heavier than the electrodes. This is virtually impossible. However, FEM simulations predicted that the frame region optimization method is not very sensitive to the exact configuration of the layer stack in the external region. It could be possible to check whether a recessed region can be designed to provide 1-D motion in the internal region without any modification of the external region but this is beyond the scope of this paper.

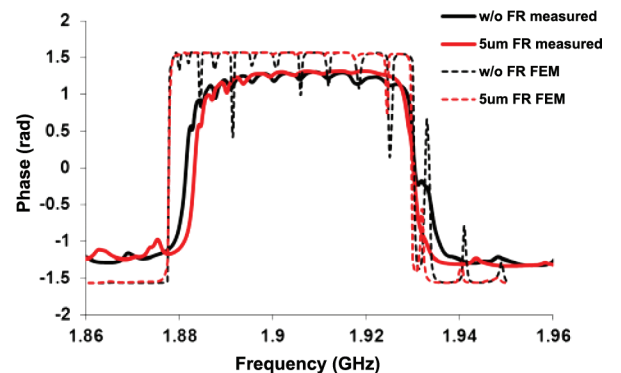


Fig. 9. Comparison of phase curves obtained from measurements (drawn lines) and the Comsol model (dashed lines) in an SMR with an optimized reflector stack with and without an FR of  $5 \mu\text{m}$ . The spurious resonances near the anti-resonant frequency are suppressed with the optimized frame region width both in the simulations and in the measurements.

The methodology, as described earlier, also assumes the displacement profiles in the internal region to be the same for the whole resonator series. Furthermore, it assumes that the displacement profile in the frame region repeats in each section of  $\lambda/4$  wide (apart from a sign). Finally, the displacement profile of the external region is the same (apart from a sign) for the whole series.

For the shear confinement to work, FR does not need to be exactly QW but only nearly QW, which can be obtained by the optimization method described in Section III. This method does not guarantee a complete suppression of spurious resonances or enhancement of the coupling coefficient which is expected in the flat amplitude mode. This could be achieved by further tailoring the layers in the external region and then adapting the optimization method. Nevertheless, that is not the focus of this work.

In FEM simulations, we have observed shear energy scaling also in a longitudinal quarter-wave reflector stack with careful choice of material properties that reflect shear waves significantly enough for the confinement. If the reflector had poor reflection properties for shear waves, then the shear-wave energy stored in this spot would have leaked into the substrate. However, the shear energy scales with odd multiple of quarter-wave frame regions once the shear energy is confined in the area under frame region.

The frame region optimization methodology is efficient for its computational time, its ease of calculating the dispersion curves, and its straightforward calculations of quarter-wave width. On the other hand, it comes to its limits when the mass loading by the frame region is so heavy (for, e.g., heavy metal frame regions) that the fundamental mode frequency of the resonator comprising an FR and ER decreases greatly. In this case, to match the frequency of that particular resonator (FR + ER) to a resonator comprising an IR and ER only, the higher order eigenfrequencies are needed which are not well resolved in Comsol FEM simulations. When the width becomes comparable to its thickness, FEM eigensimulations give mixed modes for higher orders. Extrapolating the dispersion curve of the FR + ER resonator with few initial eigenfrequencies can help, but it often introduces greater inaccuracies in the subsequent multiple FR width when scaling. Hence, accurate determination of higher order eigenmodes is essential because the FR optimization is very sensitive to eigenfrequencies.

In the reflector stack optimization methods [2], [4], [15], the enhancement in  $Q$ -factor is claimed as a consequence of the improvement in shear transmission. However, it would be additionally supportive if shear wave transmission can be extracted experimentally. The interferometry technique can only measure out-of-plane motion (vertical displacement), and hence only vibration amplitude of the longitudinal waves. Consequently, even the interferometry techniques fail to measure the amplitude of shear waves directly. With this insight of shear energy scaling, the main challenge is to explore this knowledge to carry out further studies in this direction for any possibility of shear transmission extraction.

## V. CONCLUSIONS

We have reported for the first time an alternative purpose of the optimized quarter-wave frame region; i.e., to control the shear confinement in the resonator. In addition, we report a novel methodology to suppress the spurious resonances in SMRs which is based on the formation of the dispersion curve. Usefulness of eigenfrequency simulations to obtain an optimum frame region width has been verified experimentally. Because the optimization method is straightforward, its use is facilitated also in other kinds of BAW devices, such as FBARs, lateral BAWs, and so on. The idea of shear energy scaling can be a good starting point to experimentally extract the shear wave transmission.

## ACKNOWLEDGMENTS

The authors thank Dr. A. B. M. Jansman (NXP Research, Eindhoven) for the fruitful discussions and for sharing insights on the quality factor model. Special thanks are given to the former BAW team of NXP Research, The Netherlands, especially Dr. J. Ruigrok, for the valuable discussions on Comsol simulations. Thanks are also due to S. Smits (MESA+, University of Twente) for the simulation support.

## REFERENCES

- [1] H. P. Loebl, C. Metzmacher, R. F. Milsom, P. Lok, F. van Straten, and A. Tuinhout, "RF bulk acoustic wave resonators and filters," *J. Electroceram.*, vol. 12, no. 1-2, pp. 109-118, 2004.
- [2] S. Marksteiner, J. Kaitila, G. G. Fattinger, and R. Aigner, "Optimization of acoustic mirrors for solidly mounted BAW resonators," in *Proc. IEEE Int. Ultrasonics Symp.*, 2005, pp. 329-332.
- [3] S. Marksteiner, G. G. Fattinger, R. Aigner, and J. Kaitila, "Acoustic reflector for a BAW resonator providing specified reflection of both shear wave and longitudinal waves," U.S. Patent 6933807 B2., Aug. 23, 2005.
- [4] J. W. Lobeek, R. Strijbos, A. B. M. Jansman, N. X. Li, A. B. Smolders, and N. Pulsford, "High- $Q$  BAW resonator on Pt/Ta<sub>2</sub>O<sub>5</sub>/SiO<sub>2</sub>-based reflector stack," in *Proc. IEEE Microwave Symp.*, 2007, pp. 2047-2050.
- [5] R. Strijbos, A. B. M. Jansman, J. W. Lobeek, N. X. Li, and N. Pulsford, "Design and characterization of high- $Q$  solidly-mounted bulk acoustic wave filters," in *Proc. IEEE Electronic Components and Technology Conf.*, 2007, pp. 169-174.
- [6] S. Jose, R. J. E. Hueting, and A. B. M. Jansman, "On the rule of thumb for flipping of the dispersion relation in BAW devices," in *Proc. IEEE Int. Ultrasonics Symp.*, Oct., 2011, pp. 1712-1715.
- [7] R. Aigner, "MEMS in RF filter applications: Thin-film bulk acoustic wave technology," *Sens. Update*, vol. 12, no. 1, pp. 175-210, 2003.
- [8] R. Ruby, "Review and comparison of bulk acoustic wave FBAR, SMR technology," in *Proc. IEEE Int. Ultrasonics Symp.*, 2007, pp. 1029-1040.
- [9] K. Kokkonen, T. Pensala, and M. Kaivola, "Interferometric measurements of dispersion curves and transmission characteristics of the acoustic mirror in thin film BAW resonator," in *Proc. IEEE/MTT-S Int. Microwave Symp.*, 2007, pp. 2071-2074.
- [10] K. Kokkonen, T. Pensala, and M. Kaivola, "Dispersion and mirror transmission characteristics of bulk acoustic wave resonators," *IEEE Trans. Ultrason. Ferroelectr. Freq. Control*, vol. 58, no. 1, pp. 215-225, 2011.



- [11] J. Kaitila, M. Ylilammi, J. Ella, and R. Aigner, "Spurious resonance free bulk acoustic wave resonators," in *Proc. IEEE Ultrasonics Symp.*, 2003, pp. 84–87.
- [12] J. Olivares, E. Wegmann, M. Clement, J. Capilla, E. Iborra, and J. Sangrador, "Assessment of solidly mounted resonators with wide-band asymmetric acoustic reflectors," in *Proc. IEEE Ultrasonics Symp.*, 2010, pp. 1677–1680.
- [13] T. Pensala and M. Ylilammi, "Spurious resonance suppression in gigahertz-range ZnO thin-film bulk acoustic wave resonators by the boundary frame method: Modeling and experiment," *IEEE Trans. Ultrason. Ferroelectr. Freq. Control*, vol. 56, no. 8, pp. 1731–1744, 2009.
- [14] A. B. M. Jansman, R. C. Stribos, J. W. Lobeek, F. W. M. Vanhelmont, J. J. M. Ruigrok, T. Pensala, and M. Ylilammi, "Application of a vibrating membrane model to bulk-acoustic-wave resonators," in *Proc. IEEE Ultrasonics Symp.*, 2007, pp. 1045–1048.
- [15] S. Jose, A. B. M. Jansman, R. J. E. Hueting, and J. Schmitz, "Optimized reflector stacks for solidly mounted bulk acoustic wave resonators," *IEEE Trans. Ultrason. Ferroelectr. Freq. Control*, vol. 57, no. 12, pp. 2753–2763, 2010.
- [16] S. Jose and R. J. E. Hueting, "Experimental investigation of dual wave optimized reflector stacks in solidly mounted bulk acoustic wave resonators," in *Proc. IEEE Int. Ultrasonics Symp.*, 2011, pp. 1234–1237.
- [17] T. Pensala, "Thin film bulk acoustic wave devices. Performance optimization and modeling," Ph.D. dissertation, School of Science, VTT Helsinki, Finland, 2011.



**Sumy Jose** received her bachelor's degree in physics from MG University, Kerala, India, in 2002, and her master's degree in applied electronics from the National Institute of Technology (NIT), Tiruchirappally, India, in 2004. In 2005, she joined, as a project assistant, the Indian Institute of Science (IISc), Bangalore, where she has been involved in the research projects in the area of RF MEMS design. In December 2011, she received her Ph.D. degree in electrical engineering

from the Semiconductor Components group at the University of Twente, The Netherlands. In her Ph.D. research, she developed novel design approaches for optimizing the reflector stacks in bulk acoustic wave resonators. Her primary research interests include physics-based multi-domain modeling and design of acoustic and MEMS devices. She is currently with NXP Semiconductors, Nijmegen, The Netherlands.



**Raymond J. E. Hueting** (S'94–M'98–SM'06) obtained his M.Sc. (cum laude) and Ph.D. degrees in electrical engineering from the Delft University of Technology in 1992 and 1997, respectively. His Ph.D. thesis dealt with the device physics of SiGe-based heterojunction bipolar transistors.

In 1997, he joined Philips Semiconductors, Nijmegen, The Netherlands, where he worked on lateral power MOSFETs in SOI-based BCD-IC processes used for automotive and audio applications.

He joined the Philips Research laboratories in Eindhoven, The Netherlands in 1998, and in Leuven, Belgium, in 2001, where he worked on device physics of trench-gate power MOSFETs, used for power supplies and automotive applications, and was involved in the development of novel silicon devices, among which SiGe-based heterojunction devices. Since December 2004, he has been working at the Electrical Engineering Department of the University of Twente, The Netherlands, in the field of semiconductor device physics and modeling.

Dr. Raymond J. E. Hueting authored or coauthored more than 60 papers and more than 60 patents, including 34 U.S. patents. He participates in and participated in the technical program committees of the ESSDERC and the ISPSD conferences, respectively.